Polymers **Hot Paper**

Lactone Backbone Density in Rigid Electron-Deficient Semiconducting Polymers Enabling High n-type Organic Thermoelectric Performance

Maryam Alsufyani,* Marc-Antoine Stoeckel, Xingxing Chen, Karl Thorley, Rawad K. Hallani, Yuttapoom Puttisong, Xudong Ji, Dilara Meli, Bryan D. Paulsen, Joseph Strzalka, Khrystyna Regeta, Craig Combe, Hu Chen, Junfu Tian, Jonathan Rivnay, Simone Fabiano, and Iain McCulloch*

Abstract: *Three lactone-based rigid semiconducting polymers were designed to overcome major limitations in the development of n-type organic thermoelectrics, namely electrical conductivity and air stability. Experimental and theoretical investigations demonstrated that increasing the lactone group density by increasing the benzene content from 0 % benzene (P-0), to 50 % (P-50), and 75 % (P-75) resulted in progressively larger electron affinities (up to 4.37 eV), suggesting a more favorable doping process, when employing (N-DMBI) as the dopant. Larger polaron delocalization was also evident, due to the more planarized conformation, which is proposed to lead to a lower hopping energy barrier. As a consequence, the electrical conductivity increased by three orders of magnitude, to achieve values of up to 12 S cm and Power factors of 13.2 $\mu Wm^{-1} K^{-2}$ were thereby enabled. These findings present new insights into material design guidelines for the future development of air stable n-type organic thermoelectrics.*

Introduction

Energy harvesting with conjugated polymers (CP) is most obviously exemplified in organic photovoltaics (OPVs), to enable high throughput production of flexible solar energy converters for clean energy generation.[1] Recently, conjugated polymers (CP) have also supported the development of emerging energy conversion technologies such as thermoelectric devices (TE), which offer direct conversion of heat into electric power without mechanical moving parts, making them compact and quiet compared with conventional heat engines.[2,3] In contrast with the widely studied inorganic alloys, organic polymers have significant attraction as thermoelectric materials due to their low thermal conductivity (κ), necessary for efficient energy conversion as defined by the thermoelectric Figure-of-merit ZT $=$ S2σT/κ, where S is the Seebeck coefficient, σ is the electrical conductivity and T is the absolute temperature.[3a,4] Moreover, the incorporation of solution-processable, flexible, and non-toxic conjugated polymers offer thermoelectric devices with great potential for the next generation of low-cost wearable heating/cooling devices, and near-room-temperature energy generation.[3a] Such features are impractical for toxic, rigid, and high temperature functioning inorganic materials.[5] Nonetheless, achieving high Seebeck coefficients (S) and electrical conductivities (σ) remains a challenge for organic thermoelectrics (OTEs), leading to lower than average thermoelectric (TE) performance. The development of higher performing organic thermoelectric (OTE) materials is thus essential to encourage their widespread utility.

While several p-type polymer thermoelectrics (OTE) are leading the field with electrical conductivities of > 1000 S cm^{-1} and power factors (PF $=$ S2σ) of > 100 $\mu Wm^{-1} K^{-2}$,[6] the highest performing n-type materials trail behind these values, mainly due to lack of air instability.[7] As such, the quest for high performing n-type polymers becomes key for further development of the organic thermoelectric (OTE) field. Since the Seebeck coefficients (S) of p- and n-

[*] M. Alsufyani, J. Tian, Prof. I. McCulloch
Department of Chemistry, University of Oxford
Oxford, OX1 3TA (UK)
E-mail: Maryam.alsufyani@chem.ox.ac.uk
Iain.mcculloch@chem.ox.ac.uk

M. Stoeckel, Prof. S. Fabiano
Department of Science and Technology, Linköping University
60174 Norrköping (Sweden)

X. Chen, R. K. Hallani, K. Regeta, C. Combe, H. Chen,
Prof. I. McCulloch
Physical Science and Engineering Division, King Abdullah University
of Science and Technology (KAUST)
Thuwal, 23955-6900 (Saudi Arabia)

K. Thorley
Department of Chemistry, University of Kentucky
Lexington, KY 40506-0055 (USA)

Y. Puttisong
Department of Physics, Chemistry and Biology, Linköping University
58183 Linköping (Sweden)

X. Ji, D. Meli, B. D. Paulsen, Prof. J. Rivnay
Department of Biomedical Engineering, Department of Materials
Science and Engineering, Northwestern University
2145 Sheridan Road, Evanston, IL 60208 (USA)

J. Strzalka
X-Ray Science Division, Argonne National Laboratory
Lemont, IL 60439 (USA)

Prof. J. Rivnay
Simpson Querrey Institute, Northwestern University
Chicago, IL 60611 (USA)

Supporting information and the ORCID identification number(s) for
the author(s) of this article can be found under:
https://doi.org/10.1002/anie.202113078.

type polymeric materials are comparable, approaching values of $|40–200|$ $\mu V K^{-1}$ at their maximum power factors (PFs),[8] optimizing the electrical conductivity (σ) has been the focus of many studies towards improving the thermoelectric performance of n-type polymers.[7d,9] Currently, naphthalene-tetracarboxylic diimide (NDI) based polymers, specifically N2200, are the most widely investigated n-type polymers for organic thermoelectrics, yet exhibit electrical conductivity (σ) of only 8×10^{-3} Scm^{-1} and power factor (PF) of 0.6 μWm^{-1} K^{-2}.[9c] This is firstly ascribable to interchain charge localization observed in N2200 and related donor-acceptor (D-A) polymers,[9b,10] which arises from large torsional angles between the donor and acceptor units, combined with the inefficient n-doping of the donor unit, due to its poor electron accepting ability.[7a,e,11] Theoretical and experimental investigations reveal that the HOMO and LUMO orbital coefficients of (D-A) polymers are localized on the donor and acceptor moieties, respectively, and the negative polaron of the n-doped polymer is localized only on the acceptor unit.[9e,11a,12] These indications suggest that the inactive n-doping of the donor unit together with the respective orbital energies of the donor and acceptor units have a significant impact in charge localization reported for N2200 and several other (D-A) polymers, ultimately limiting their carrier mobility and conductivity.[9b] Inducing charge delocalization along the polymer backbone has been the focus of a myriad of studies by i) boosting a more planarized structures[9e,13] and ii) reducing the donor character of the traditional (D-A) polymers.[7e,14] The ladder-type polymer, polybenzimidazo-benzophenanthroline (BBL) provides a good example to highlight the significance of a planarized rigid backbone in overcoming this limitation, reaching electrical conductivity (σ) up to 3 orders of magnitude larger, and power factor (PF) of 1 order of magnitude higher than N2200, which suggests a higher polaron mobility.[9e] Furthermore, a recent study demonstrated that enhancing backbone planarity together with minimizing (D-A) character help overcome the columbic interaction between polymer and dopant, reducing the number of free charges and subsequently the doping efficiency.[15]

Secondly, the modest performance of N2200 is also ascribed to the poor miscibility between the host polymer and employed dopant.[16] Such extrinsic limitation has been resolved by a number of related studies, such as increasing the side chains polarity by utilizing ethylene glycol oligomeric derivatives, which results in an improved dopant dispersion in the polymer matrix, as compared to the traditional alkyl side

chains, leading to several fold enhancement in electrical conductivities (σ) and subsequent thermoelectric performance.[9d,17]

We hypothesized that molecular engineering of conjugated polymers exhibiting rigid backbone with all acceptor (A-A) properties and polar side chains, will be beneficial in achieving high performing n-type organic thermoelectric devices. These rigid polymers exhibit excellent thermal stability, imperative for thermoelectric applications.[18] Enhanced dopant/polymer mixing imparted by the use of glycol-based side chains is expected, which crucially affects the doping process, and subsequently the thermoelectric performance. All electron deficient backbone polymers will also exhibit high electron affinity due to the electron withdrawing accepting functional groups, thus enabling a thermodynamically favorable n-doping mechanism that is also essential for facile n-doping in the presence of oxygen and water and thus for achievement of air-stable n-organic thermoelectrics.[19]

Few electron deficient rigid polymers have been reported with thermoelectric performance reaching power factor (PF) milestones of the order of $10^{0–1}$ μWm^{-1} K^{-2}.[7c,9e,13] Nonetheless, considering that in most organic thermoelectric studies, the electrical conductivity (σ) is the main parameter to improve, values above 10 S cm^{-1} have been scarcely reported for n-type conjugated polymers.[7c,d,9a] We believe that this is due to the insufficient studies giving structural design guidelines to optimize device performance.[13,14,17a]

We demonstrate judicious molecular design of electron deficient fused lactone-based polymers to optimize thermoelectric performance. A series of three co-polymers containing benzene and naphthalene building blocks were synthesized, exhibiting a rigidified structure. The backbone conformation has been planarized by the double bonds imparted by a simple aldol condensation of enolic bis-lactone and electrophilic bis-lactam electron-withdrawing units. We sought to use a mixture of alkylated and glycolated solubilizing components to balance self-assembly, aggregation and dopant compatibility, ultimately affording the co-polymers P-0, P-50, and P-75. Polymer structures are illustrated in Figure 1. We explore the effect of aromatic size core on controlling the electron deficiency and the overall organization of the polymers, which impacts the thermoelectric performance. Upon optimized doping conditions, P-75 with the highest number of benzene core, and therefore the highest lactone density, displays the largest electrical conductivity (σ) of 12 Scm^{-1} and power factor (PF) up to 13.2 μWm^{-1} K^{-2}. The conductivity of P-75 is significantly higher than that of other
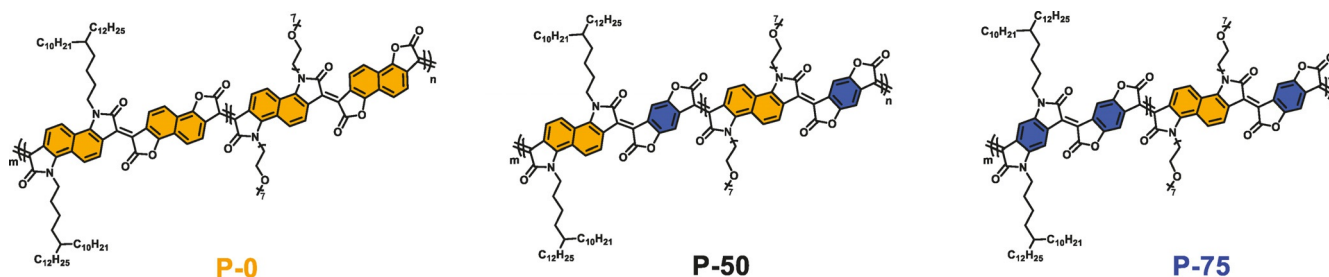
Figure 1. Chemical structures of the lactone based-rigid polymers investigated herein.

doped (A-A) and (D-A polymers),[7a–c,e,13a] and one of the few reported n-type polymers displaying an electrical conductivity value over 10 S cm⁻¹.[7c,d,9a,20] Its power factor is also among the highest reported for solution processable n-type thermoelectric polymers. Our work demonstrates the critical role of aromatic ring size optimization in successful n-doping of the attractive all-acceptor rigid conjugated polymers and provide future material design guidelines for the advancement of n-type organic thermoelectrics.

Results and Discussion

All monomers were synthesized according to literature procedures.[21] Firstly, benzene-bis-isatin (M1) is prepared by oxidizing cyclohexanedione in ethanol, followed by amination and aromatization in the same reaction vessel. The corresponding diamine undergoes acylation, followed by ester hydrolysis. Swern oxidation of the intermediate dialcohol produces a diglyoxamide, prior to a Pummerer cyclisation. Oxidation of the resulting tricyclic intermediate yields benzene- bis-isatin (M1) in 25 % yield. Second, synthesis of the naphthalene-bis-isatin monomers (M2) and (M3) followed a Martinet dioxindole condensation approach, by reacting 1,5-diaminonapthalene with diethyl ketomalonate form the bis-oxindole intermediate, which was then oxidized to form the bis-isatin. The subsequent n-alkylation/n-glycolation has afforded (M2) and (M3) in 20 % yield. Preparation of benzo-difuran monomer begins with a nucleophilic addition of 1,4-benzoquinone by ethyl cyanoacetate, followed by a hydrolysis to generate the diacid intermediate, which is subsequently dehydrated with acetic anhydride to yield 30 % of the benzo-difuran monomer (M4). Lastly, naphtha-difuran monomer was obtained via the addition of 1,1,2-trichloroethyelene to the 1,5-dihydroxynaphthalene to generate dichlorovinyl-oxynaphthalene intermediate. Following that, an elimination step with *n*-BuLi has afforded the dialkyne, which was subjected to an oxidative cyclization procedure to provide (M5) in 10 % yield.

Polymers P-0, P-50 and P-75 were synthesized using the previously reported metal-free polymerization[21a] where an acid catalyst is employed to drive the aldol condensation between the enolic and electrophilic carbonyl units of bis-lactone and bis-isatin building blocks. This metal-free approach offers numerous advantages over transition-metal mediated reactions (such as Stille, Suzuki–Miyaura, or Kumada coupling), in which metal reagents can be costly and highly toxic. Furthermore, having water as the only byproduct provides aldol condensation with no arduous purification steps that accompanies the use of metals such as palladium. Ultimately, P-0, P-50, and P-75 were obtained with number-average molecular weights (Mn) of 10 (k)gmol⁻¹, 10.7 (k)gmol⁻¹, and 18 (k)gmol⁻¹. Detailed polymeri-

zation conditions are reported in the supporting information (Section 2.3). Unfortunately, the synthesis of the P100 extension of this series was synthetically unattainable via the Martinet dioxindole condensation route. This route requires the synthesis of a glycolated benzo-bis-isatin comonomer, which, under our conditions, was not isolable.

The thermal properties of P-0, P-50, and P-75 can be found in Figure S18. All polymers showed excellent thermal stability with a decomposition temperature of over 350 °C, as determined by thermogravimetric analysis (TGA) and no phase transitions in the range from room temperature to 300 °C were observed by differential scanning calorimetry (DSC) for P-0. Conversely, P-50 exhibits a heating endotherm peak around 102 °C and a cooling exothermic peak at 64 °C. P-75 exhibits endothermic and exothermic peaks at 142 °C and 120 °C, with a slightly increased peak intensity. The same peaks were observed in the second cycle for both polymers. The thermal transition behavior suggests a more ordered structure of the benzene-containing polymers, P-50 and P-75, than the all-naphthalene derivative P-0.

The ionization potential (IP), the electron affinity (EA) and optical gap (Eg) of the polymers were determined by a variety of spectroscopic techniques including photo electron spectroscopy in air (PESA), thin-film absorption spectra (UV-VIS-NIR), ultraviolet photoelectron spectroscopy (UPS), and low energy inverse photoelectron spectroscopy (LE-IPES). The corresponding data are listed in Table 1. P-75 showed the largest ionization potential (IP) and electron affinity (EA) of 5.30 and 4.37 eV, respectively, one of the largest reported electron affinities among glycolated n-type semiconducting polymers, which is attributed to the high density of the electron-withdrawing carbonyl groups. As the lactone content is reduced by reducing the benzene core to 50 % in P-50, the ionization potential (IP) and electron affinity (EA) slightly decreased to 5.29 and 4.30 eV. The all naphthalene derivative P-0 has considerably exhibited the smallest ionization potential (IP) and electron affinity (EA) of 5.21 and 4.09 eV. This is chiefly attributed to the effective dilution of the electron withdrawing group density (C=O) along the conjugated backbone, by increasing the size of the aryl ring and consequently rendering the benzene free backbone (P-0) less electron deficient compared with its lactone- benzene-containing counterparts P-50 and P-75. Additionally, introducing more benzene content has been shown to reduce the backbone twisting (discussed later in the

Table 1: Polymers physical and electrical properties.

Polymer	Mn/Mw [(k)gmol⁻¹]	PDI	IP[a] [eV]	EA[a] [eV]	Eg[a] [eV]	IP[b] [eV]	EA[b] [eV]	Eg[b] [eV]	λmax,film[c] [nm]	IP[d] [eV]	EA[d] [eV]	Eg[d] [eV]
P-0	10 K/14 K	1.4	5.69	3.44	2.25	5.55	4	1.55	823	5.21	4.09	1.12
P-50	10.7/14 K	1.3	5.72	3.61	2.11	5.55	4.2	1.35	973	5.29	4.30	0.99
P-75	18/33 K	1.8	5.77	3.68	2.09	5.55	4.3	1.25	998	5.30	4.37	0.93

[a] Calculated by Density Functional Theory (DFT) simulations. [b] IP is measured by ultraviolet photoelectron spectroscopy (UPS) and EA by low energy inverse photoelectron spectroscopy (LE-IPES). [c] Thin films were spin-cast on glass substrates from chloroform solution; λ is the peak of the first low energy absorption band of the polymers. [d] Estimated optical gap calculated using onset of absorption spectra (E$_{opt.gap}$ = 1240/λ$_{onset}$), IP is measured by photo electron spectroscopy in air (PESA) and EA is calculated from E$_{opt.gap}$ and IP.

theoretical modelling section) and increase the pi orbital overlap along the backbone which leads to a narrowing of the band gap to 0.93 eV for P-75. The optical band gap widens with reducing benzene content in P-50 and P-0 to reach 0.99 and 1.12 eV, respectively. Moreover, these lactone-based polymers exhibited lower LUMO levels than analogous previously reported lactam fused polymers,[13b] suggesting greater electron-withdrawing properties of the lactone functional group, when compared with lactam groups, thus higher electron affinities are achieved.

The doping behavior of the three polymers were studied by UV-vis-NIR absorption spectroscopy and electron paramagnetic resonance (EPR) spectroscopy. The corresponding absorption spectra can be found in Figure 2 a–c. In the pristine state, all polymers exhibit three absorption peaks. Two absorption bands with maximum absorption wavelength (λ_{max}) at (467 and 652 nm for P-0), (497 and 631 nm for P-50) and (516 and 658 nm for P-75). The onset absorption wavelength for P-0, P-50, and P-75 are 1107, 1252, and 1333 nm, respectively. P-0 exhibits a shorter onset absorption wavelength than P-50 and P-75. This is consistent with its wider optical band gap, resulting from the reduced pi orbital overlap upon backbone twisting. The dopant N-DMBI, (4-(1, 3dimethyl2, 3-dihydro-1*H*-benzoimidazol-2-yl)phenyl)dimethylamine) was selected to solution-dope all the polymers due to its reported strong n-doping ability for various n-type semiconductors,[7c, 9c, 22] high chemical stability, and good solution processability.[22b]

Moreover, its shallow SOMO energy level of (−2.8 eV) offer an effective energy offset with the polymers in this study, which is necessary for electron transfer from the donor (N-DMBI) to the host polymers.[23] As shown in Figure 2 a–c,

upon doping the three polymers with N-DMBI, the neutral absorption features in the spectrum region at 400–700 nm sharply decrease in intensity. The n-doping is concurrently accompanied by the rising of a new absorption band at 1100–1200 nm, which we attributed to polarons, and one in the IR region at wavelength > 1500 nm, which we ascribed to bipolarons. Furthermore, 50% and 100% doping of P-75 is accompanied with full quenching of the pristine polymer peaks and a more pronounced appearance of bipolaron peaks, which could be the cause for the decreased charge carrier mobility and therefore the conductivity at 100% doping ratio, as will be discussed later.

To shed light on the doping process, the pristine and doped polymers at various doping level were evaluated by electron paramagnetic resonance (EPR) spectroscopy. Bipolarons are EPR silent, whereas polarons are unpaired electrons that are EPR active. Interestingly, as demonstrated in Figure 2 d–f, all pristine polymers showed EPR signals, suggesting the existence of an intrinsic charge density in the pristine (undoped) polymers. While the origin of this intrinsic charge density remains elusive, we note that it has already been observed for similar lactone polymers and tentatively ascribed to diradicals.[13a] The spin density is relatively weak for pristine P-0, and it enhances upon doping, indicating the generation of polaronic species as shown in Figure 2 d. In contrast to P-0, P-50 and P-75 displayed a different spin behavior, with a relatively strong spin density of the undoped polymers that considerably decreases upon doping. We tentatively attribute this observation to the formation of EPR-silent bipolarons.

The polymers were investigated by grazing-incidence wide-angle X-ray scattering (GIWAXS) to gain insight into
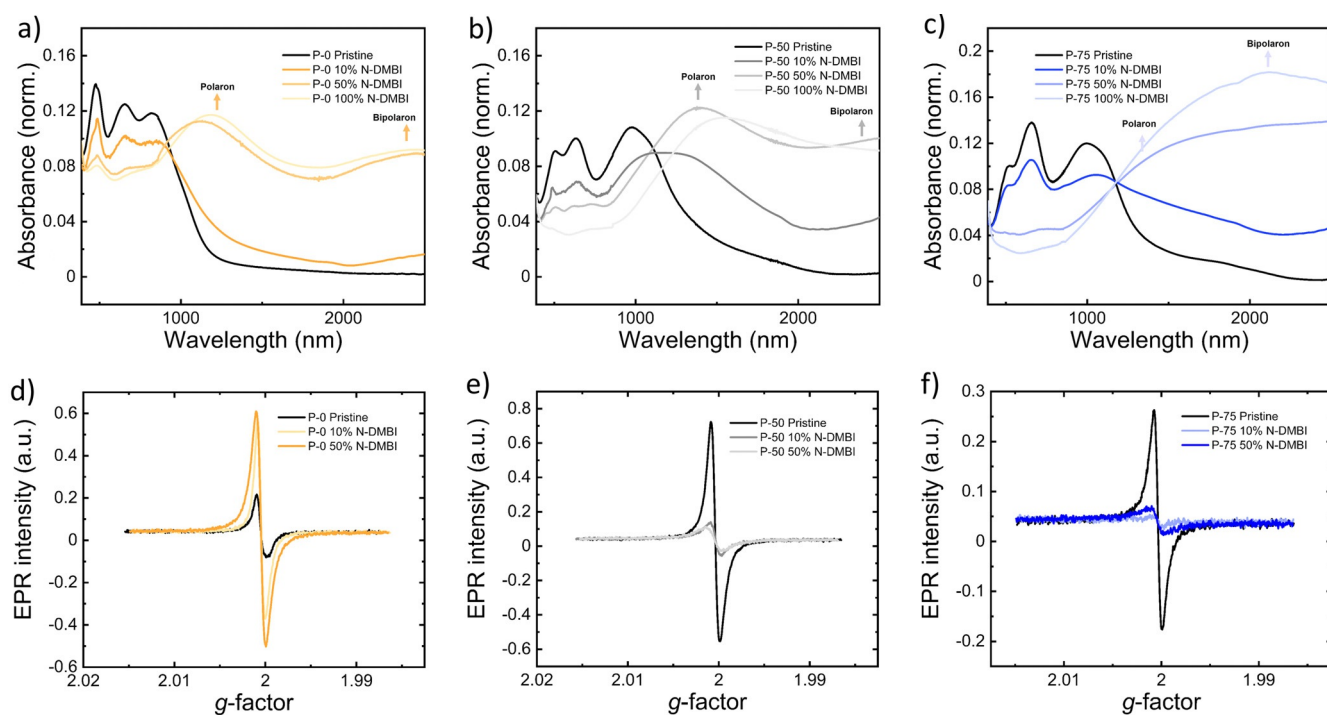
Figure 2. UV-vis-NIR thin film absorption spectra of the pristine and doped a), b) P-50, and c) P-75. EPR signals of the pristine and the doped d) P-0, e) P-50, and f) P-75.
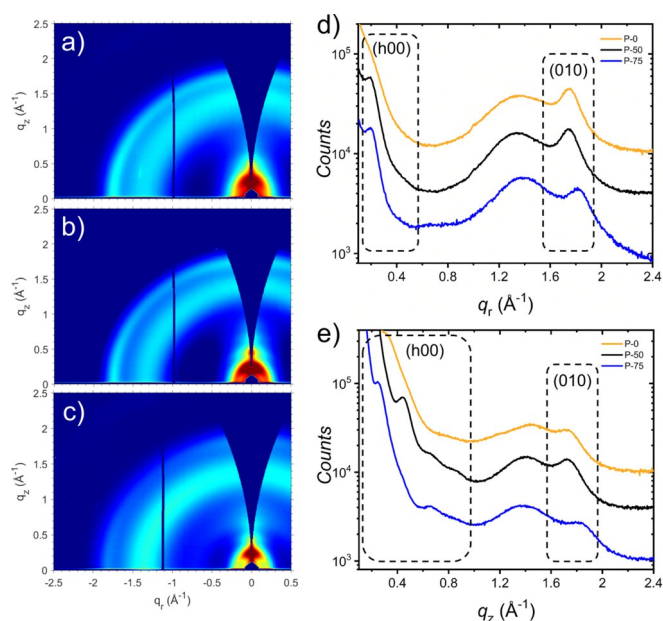
Figure 3. GIWAXS Patterns: Two-dimensional grazing incidence X-ray scattering map of (a) P-0, (b) P-50, and (c) P-75. GIWAXS Linecuts. (d) In-plane (q_r) and (e) out-of-plane (q_z) scattering line cuts from P-0, P-50, and P-75 (offset in intensity for clarity) highlighting the lamellar (h00) and π-stack (010) scattering.

their thin film. The two-dimensional scattering patterns and in- and -out-of-plane line cuts are illustrated in Figure 3. All three polymers showed nominally similar scattering patterns in line with the previously reported analogues, though with diminished degrees of lamellar scattering.[13a,14a] As shown in 2D GIWAXS, all three polymers show a strong isotropic amorphous scattering ring centered near 1.4 Å-1, with lamellar stack (h00) and π–π stack (010) scattering present both in- and out-of-plane. The π–π stack (010) scattering transitioned from mostly isotropic in P-0 to a mix of largely in- and out-of-plane for P-75, with P-50 presenting an intermediate case.

This shows that the reduction of the naphthalene rings in the backbone drives the otherwise randomly aligned crystallites into a preference for edge- or face-on texture, which is correlated with the improved thermoelectric performance. As seen in Figure 3 a-c, the lamellar (h00) scattering was not well resolved against the scattering background, indicating a relatively diminished population of scatterers, which increases the uncertainty in calculated d-spacings and crystallite coherence lengths (Lc), see Table S1. This is especially true in the case of P-0 which shows only weak scattering shoulders and no evidence of higher ordered scattering peaks/shoulders. In the case of P-50 and P-75, the lamellar stacking appeared tighter out-of-plane than in-plane, and in-plane coherence lengths were roughly equivalent. In general, the π–π stack (010) scattering was better resolved. P-0 showed the largest π–π stack coherence lengths in- and out-of-plane, however, the thermoelectric performance did not correlate with simple coherence length. The π–π stack d-spacings of P-0 and P-50 were very similar ($\approx$3.6 Å) both in- and out-of-plane. P-75 however showed a significantly tighter π–π stack d-spacings

3.45 and 3.41 Å in- and out-of-plane, respectively. The P-75 π–π stack d-spacing was tighter than previous analogues as well.[13a,14a] and correlated with improved thermoelectric performance.

To investigate the effect of doping on the polymer's surface morphology, atomic force microscopy (AFM) was carried out, Figure S21. All pristine polymers form smooth thin films with roughnesses below 1 nm. Interestingly, after 10% doping with N-DMBI, the polymers thin films display uniform morphologies. Unlike PCBM and N2200 with high crystallinity,[9c,22b] N-DMBI doped thin films of P-0, P-50 and P-75 present negligible particles and aggregates on the top of the surface. The low crystallinity of the three polymers indicate greater dopant dispersion in polymer films, resulting in a more efficient doping process. Higher content of N-DMBI leads to segregation at the surface of the three polymers, which congruent with the decreased thermoelectric performance at high doping concentrations.

To examine the effect of lactone maximization on the conformation of the backbone, oligomers of P-0, P-50, and P-75 were modeled by density functional theory (DFT) simulations. The long solubilizing alkyl and glycol chains were reduced to methyl groups to simplify the simulations. Firstly, the double bond connection appears to significantly reduce the twist angle between the building blocks, with torsional potential energy surfaces showing an energetic minimum at 160°, suggesting a conformationally locked backbone of the three polymers, Figure S25. P-0, P-50, and P-75 exhibit dihedral angle average of ±20.1°, ±18.5°, and ±14.9°, respectively. The observed reduction in dihedral angle from P-0 to P-75 establishes an indication that increasing the lactone unit through benzene maximization has an influence on reducing the torsional angle between the building blocks and thus backbone planarization. This in turn ought to anticipate P-75 with stronger orbital overlap, extended polaron delocalization and hence an improved charge carrier transport.

We are particularly interested in investigating the negative polaron distribution, given its crucial impact on charge mobility and thereby electrical conductivity. Charge distribution analysis was performed on the density functional theory calculations using Hirshfeld charges, which has previously used to model polaron species of polymers.[24] In short, the Hirshfeld analysis partitions the electron density to allocate a partial charge to each atom. These charges are summed for the atoms making up the different lactone or lactam repeat fragments, such that the spread of charge in the radical anion can be visualized along the polymer chain, and the contributions of the different functional groups and naphthalene/ benzene rings to charge stabilization can be observed. Figure 4 d), e) and f) illustrates the negative polaron distribution on the alternating lactone and lactam units, where (orange, black and blue bars represent lactone unit, and gray bars represent lactam unit). Additionally the napthalene-containing units are diagonally shaded, whereas the benzene rings are not. Figure 4 d) shows that negative polarons in P-75 were distributed to a greater extent when compared to P-50 and P-0, where the negative charges reside on three fragments (3–4–5) for P-50 and only two fragments (4–5) for P-0. To show
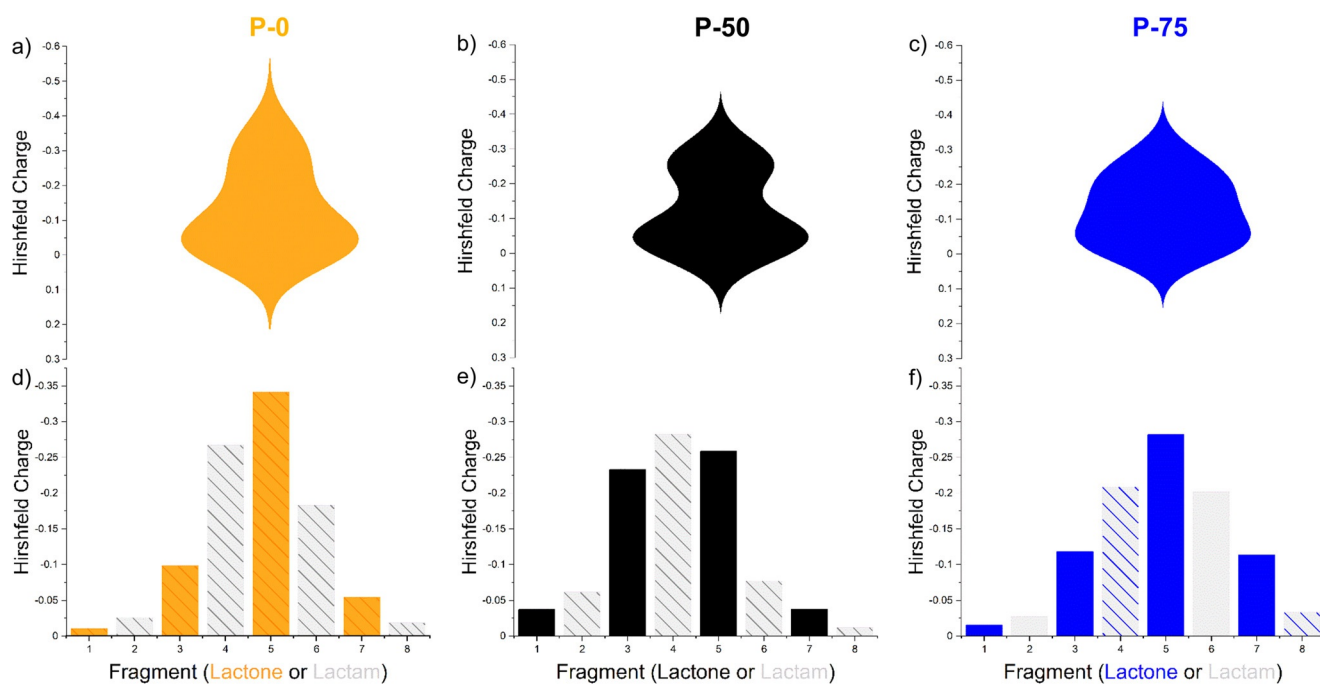
Figure 4. The illustrative symmetric violin plots smoothed by Kernel density a) P-0, b) P-50, and c) P-75 of the corresponding Hirschfeld charge distribution d) P-0, e) P-50, and f) P-75 in reduced polymers based on a fragment analysis of the polymer chain. Lactam groups shown in gray, Lactone groups shown in other colors. Napthalene-containing units are diagonally shaded, whereas the benzene rings are not.

a clear comparison of the charge distribution across the polymers, Hirshfeld charges of each polymer were also demonstrated in mirrored distribution curves, also called Violin plots. As seen in Figure 4 a), b) and c), the negative polarons in P-75 appear to be more evenly distributed along the fragments, with a more uniform topology than those shown in P-50 and P-0. The charge distribution within the polymer has shown to have a substantial effect on intermolecular charge transport.[9e] whereby the increased spread of charge provides a larger surface area for charge hopping within the polymer chains, which leads to increasing the interchain carrier mobility and consequently electrical conductivity.[25] The above analysis thus suggest P-75 with a more delocalized nature of the negative polarons, which was attributed to imposing more benzene moieties to the backbone, and subsequently a higher concentration of carbonyl groups. The planarized backbone and polaron delocalization of P-75 suggest a highly efficient charge transport.

Lastly, the energy levels of the three polymers were computed with respect to the vacuum level. The calculated ionization potential (IP) values for P-0, P-50, and P-75 were 5.69 eV, 5.72 eV, and 5.77 eV, thus reflecting the same trend in the experimentally recorded data. A good fit was also observed between the experimental and simulated trends obtained for the polymer electron affinity (EA), with EA of P-75 being the largest (3.68 eV), the middle for P-50 (3.61 eV) and the smallest for P-0. (3.44 eV).

The maximum electrical conductivity values of pristine and doped polymers are plotted in Figure 5 a,b as a function of temperature. Figure 5 shows that charge transport is thermal activated in these polymers. The Arrhenius-type temperature activation energies (Eas) of pristine P-0, P-50,

and P-75 are 232, 141, and 114 meV, and drop to 174, 78, and 60 meV, respectively, after doping at 10 mol% of N-DMBI. Upon doping, the decrease in activation energy is ascribed to
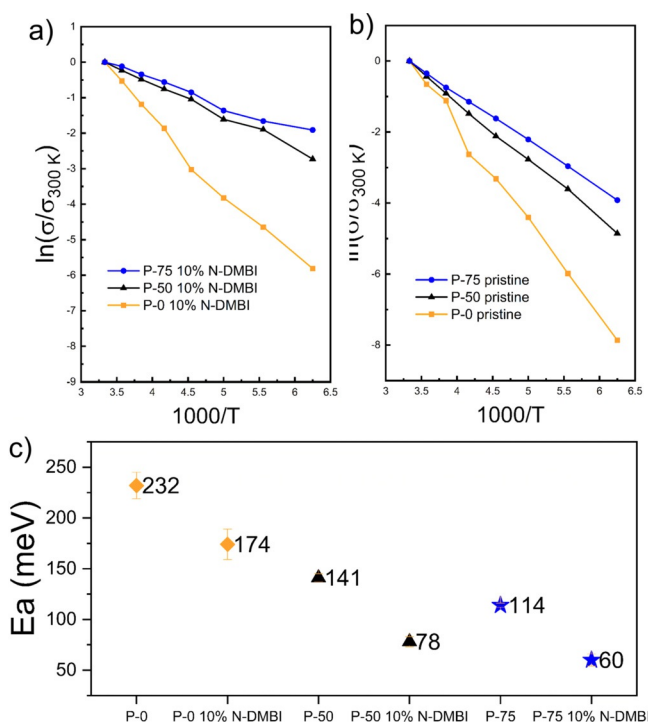

Figure 5. The Arrhenius plot of the temperature dependent electrical conductivity of a) pristine and b) doped polymers, measured in 4-probes configuration. C) the extracted activation energy displaying the trend of decreasing the hopping barrier from P-0 to P-75.

the filling of trap states near the conduction levels due to the increased number of charge carriers generated by N-DMBI.[26] A doping level of 10 mol % has been selected because it matches the highest conductivity observed for P-75, as a higher percentage of dopant would lead to perturbation of the polymer morphology due to dopant aggregation.[27] These results suggest the trend of the hopping barrier in the pristine and doped films follows: P-75 < P-50 < P-0. The large difference in the hopping activation energy implies that as the benzene-lactone unit is maximized in P-75, the number of free charges increases, due to the enhanced backbone planarization and electron-deficiency, which in turn allow i) easier dissociation of the columbic interaction between the dopant and polymer, hence corresponds to enhanced carrier density,[15] and ii) better charge transport,[9e] where both parameters have a substantial role in improving the electrical conductivity the subsequent thermoelectric performance.

To evaluate the thermoelectric properties, the electrical conductivity and Seebeck coefficient of doped P-0, P-50, and P-75 were investigated as a function of the dopant molar concentration. As shown in Figure 6, all three polymers exhibit an intrinsic electrical conductivity. In the case of P-0, this intrinsic electrical conductivity is 3.19×10^{-5} S cm^{-1} and increases to 0.05 S cm^{-1} for P-50, reaching the considerably high value of 0.5 S cm^{-1} for P-75. The recorded intrinsic conductivities correlate well with the EPR signals of the pristine polymers, corroborating the existence of a free charge density in the pristine polymers. Upon doping with N-DMBI, the electrical conductivities dramatically rise, reaching a maximum value when the percentage of N-DMBI is 10 mol % for P-50 and P-75. At higher doping concentrations, the conductivity of P-50 and P-75 starts to decrease, possibly due to the disruption of the thin film microstructure after introducing a large number of dopants, leading to a drop in carrier mobility. P-0, on the other hand, does not feature an electrical conductivity maximum in the same dopant concentration range. For P-0, the electrical conductivity increases about three orders of magnitude from 0 to 20 % N-DMBI ratio, but only by a factor of two at dopant concentration between 20–100 %. This is ascribed to the aggregation of N-DMBI, which is known to occur at high loading concentrations.[17b] The polymers P-0, P-50, and P-75 reached maximum conductivities of 0.012, 0.76, and 12 S cm^{-1}, respectively. To the best of our knowledge, P-75 is one of the few reported n-type polymers displaying an electrical conductivity value over 10 S cm^{-1}.[7c,d,9a] These results suggest that dominant factor in conductivity optimization is energy level offset, arising from increasing the density of electron withdrawing groups along the backbone, which drives electron transfer. P-50 demonstrates an electrical conductivity four times higher than its alkylated analogue (P1), which we previously reported[14a] highlighting the effect of polar side chain on enhancing the polymer/dopant miscibility, which has proven to be beneficial for enhancing the electrical conductivity. The Seebeck coefficient values of all three polymers are negative, indicating a predominant n-type character.[28] As shown in Figure 6 b), the Seebeck coefficients of P-0, P-50, and P-75 decreases monotonously with increasing dopant concentration, due to the opposite correlation between Seebeck coefficients and charge carrier concentration. At 10 mol % DMBI, P-75 displays a Seebeck coefficient of −105 µV K^{-1}, while P-0 and P-50 have Seebeck coefficients of −213 and −61 µV K^{-1}, respectively. Finally, a combination of the electrical conductivity (σ) and Seebeck coefficient (S) yielded a maximum power factor (PF = S^{2}σ) as high as 13.2 µW m^{-1} K^{-2} for P-75, which is among the highest recorded for solution-processed n-type OTE materials. In contrast, the maximum power factor of P-50 and P-0 were only 0.29 and 0.002 µW m^{-1} K^{-2}, respectively.

The air instability of n-type thermoelectric polymers has an imperative role in limiting their widespread applications, mainly caused by the quenching of the radical anions by H$_2$O
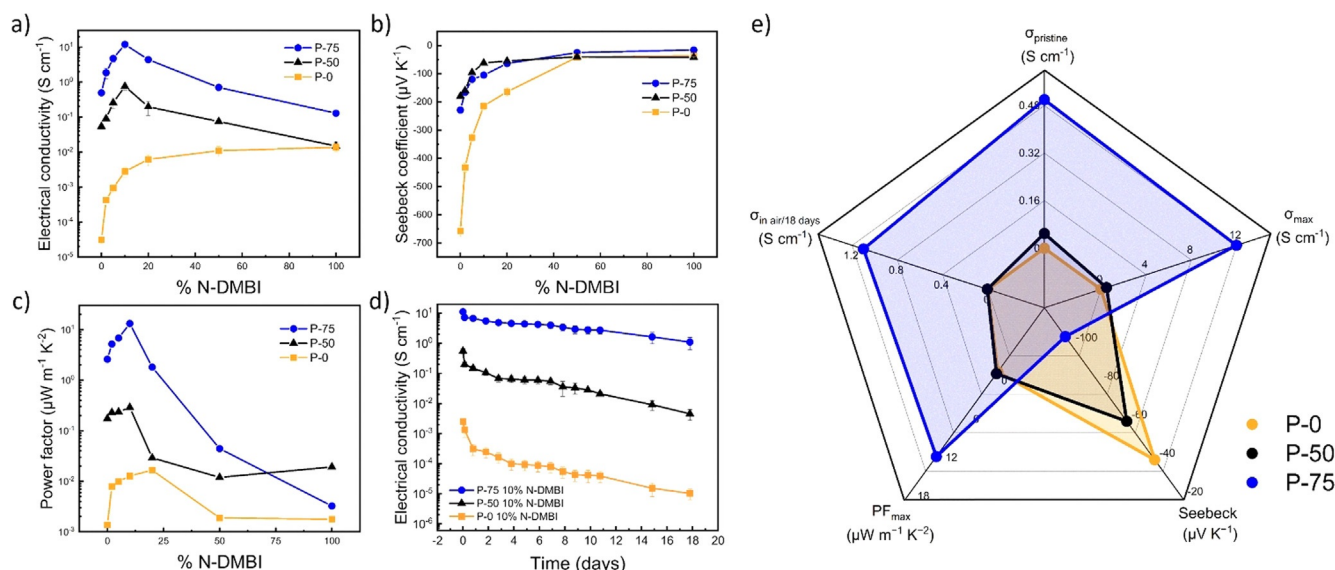
Figure 6. a) Electrical conductivities, (b) Seebeck coefficients, and (c) power factors recorded for P-0, P-50, and P-75 at different doping ratios. d) Conductivity stability of the doped polymer thin films in air. e) Radar chart illustrating the trend of thermoelectric performance of the three polymers.

and O_2 in ambient air.[29] The deep LUMO energy levels recorded with our polymers helps to effectively suppress this quenching process. Figure 6 d shows the stability of doped polymer thin films in air (thicknesses of P-0, P-50 and P-75 were 30 nm, 19 nm and 41 nm, respectively), where the electrical conductivity was monitored over 18 days. While the electrical conductivities of P-50 and P-0 drops two orders of magnitude to values of 4×10^{-3} S cm^{-1} and 1×10^{-5} S cm^{-1}, respectively, P-75 showed only one order of magnitude loss and remained at 1.2 S cm^{-1}.

Conclusion

In summary, three new lactone-based rigid semiconducting polymers were synthesized with different densities of electron withdrawing functionality along the backbone, for n-type thermoelectric application. Aldol condensation has provided the polymers with simple metal-free approach that doesn't require complex purification processes, and was also beneficial towards imposing rigidity through double bond linkage between the polymer building blocks. TGA analysis indicated excellent thermal stability of the three polymers. All polymers exhibit deep LUMO energy levels, determined both experimentally and computationally, attributed to the high density of electron-deficient lactone unit along the backbone, reaching measured electron affinities as high as 4.37 eV. Both absorption spectra and EPR signals have confirmed the successful doping of the polymers with N-DMBI. DFT theoretical modelling indicates that all polymers exhibit a locked confirmation and suggests that increasing the lactone-benzene ring density on the backbone leads to enhanced planarization and polaron delocalization, which in turn is proposed to be beneficial for electron transport and lower hopping activation barriers, necessary for high electrical conductivities. Finally, the effect of lactone group density maximization has resulted in high electrical conductivity of 12 S cm^{-1}, one of the few reported n-type polymer with such high conductivities, and subsequent high power factor of 13.2 μW m^{-1} K^{-2}, which is among the highest reported n-type thermoelectrics. The enhanced electron affinity accompanied with lactone maximization is suggested as the dominant factor in optimizing the thermoelectric performance with considerable stability in ambient conditions. The findings of this study highlight that replacing the lactam groups with the stronger electron withdrawing lactone group is an effective design strategy to optimize the thermoelectric performance, and offer new insights into material design guidelines for the future development of air stable n-type organic thermoelectrics.

Acknowledgements

Conflict of Interest

The authors declare no conflict of interest.

[1] K. A. Mazzio, C. K. Luscombe, *Chem. Soc. Rev.* **2015**, *44*, 78–90.

[2] S. LeBlanc, *Sustainable Mater. Technol.* **2014**, *1*, 26–35.

[3] a) B. Russ, A. Glaudell, J. J. Urban, M. L. Chabinyc, R. A. Segalman, *Nat. Rev. Mater.* **2016**, *1*, 16050; b) M. Massetti, F. Jiao, A. J. Ferguson, D. Zhao, K. Wijeratne, A. Würger, J. L. Blackburn, X. Crispin, S. Fabiano, *Chem. Rev.* **2021**, *121*, 12465—12547.

[4] M. Goel, M. Thelakkat, *Macromolecules* **2020**, *53*, 3632–3642.

[5] C. J. Yao, H. L. Zhang, Q. Zhang, *Polymers* **2019**, *11*, 107.

[6] a) O. Bubnova, Z. U. Khan, A. Malti, S. Braun, M. Fahlman, M. Berggren, X. Crispin, *Nat. Mater.* **2011**, *10*, 429–433; b) G.-H. Kim, L. Shao, K. Zhang, K. P. Pipe, *Nat. Mater.* **2013**, *12*, 719–723; c) Y. Xia, K. Sun, J. Ouyang, *Adv. Mater.* **2012**, *24*, 2436–2440; d) S. H. Lee, H. Park, S. Kim, W. Son, I. W. Cheong, J. H. Kim, *J. Mater. Chem. A* **2014**, *2*, 7288–7294.

[7] a) Y. Wang, M. Nakano, T. Michinobu, Y. Kiyota, T. Mori, K. Takimiya, *Macromolecules* **2017**, *50*, 857–864; b) X. Yan, M. Xiong, J. T. Li, S. Zhang, Z. Ahmad, Y. Lu, Z. Y. Wang, Z. F. Yao, J. Y. Wang, X. Gu, T. Lei, *J. Am. Chem. Soc.* **2019**, *141*, 20215–20221; c) K. Shi, F. Zhang, C. A. Di, T. W. Yan, Y. Zou, X. Zhou, D. Zhu, J. Y. Wang, J. Pei, *J. Am. Chem. Soc.* **2015**, *137*, 6979–6982; d) Y. Wang, K. Takimiya, *Adv. Mater.* **2020**, *32*, e2002060; e) C. Dong, S. Deng, B. Meng, J. Liu, L. Wang, *Angew. Chem. Int. Ed.* **2021**, *60*, 16184–16190; *Angew. Chem.* **2021**, *133*, 16320–16326.

[8] a) R. Yue, J. Xu, *Synth. Met.* **2012**, *162*, 912–917; b) D. Kiefer, R. Kroon, A. I. Hofmann, H. Sun, X. Liu, A. Giovannitti, D. Stegerer, A. Cano, J. Hynynen, L. Yu, *Nat. Mater.* **2019**, *18*, 149–155; c) H. Li, M. E. DeCoster, R. M. Ireland, J. Song, P. E. Hopkins, H. E. Katz, *J. Am. Chem. Soc.* **2017**, *139*, 11149–11157; d) C.-K. Mai, R. A. Schlitz, G. M. Su, D. Spitzer, X. Wang, S. L. Fronk, D. G. Cahill, M. L. Chabinyc, G. C. Bazan, *J. Am. Chem. Soc.* **2014**, *136*, 13478–13481; e) W. Shi, T. Zhao, J. Xi, D. Wang, Z. Shuai, *J. Am. Chem. Soc.* **2015**, *137*, 12929–12938; f) S. N. Patel, A. M. Glaudell, K. A. Peterson, E. M. Thomas, K. A. O'Hara, E. Lim, M. L. Chabinyc, *Sci. Adv.* **2017**, *3*, e1700434.

[9] a) Y. Lu, Z. D. Yu, Y. Liu, Y. F. Ding, C. Y. Yang, Z. F. Yao, Z. Y. Wang, H. Y. You, X. F. Cheng, B. Tang, J. Y. Wang, J. Pei, *J. Am. Chem. Soc.* **2020**, *142*, 15340 – 15348; b) B. D. Naab, X. Gu, T. Kurosawa, J. W. F. To, A. Salleo, Z. Bao, *Adv. Electron. Mater.* **2016**, *2*, 1600004; c) R. A. Schlitz, F. G. Brunetti, A. M. Glaudell, P. L. Miller, M. A. Brady, C. J. Takacs, C. J. Hawker, M. L. Chabinyc, *Adv. Mater.* **2014**, *26*, 2825 – 2830; d) Y.-h. Shin, H. Komber, D. Caiola, M. Cassinelli, H. Sun, D. Stegerer, M. Schreiter, K. Horatz, F. Lissel, X. Jiao, C. R. McNeill, C. Simò, C. Bertarelli, S. Fabiano, M. Caironi, M. Sommer, *Macromolecules* **2020**, *53*, 5158 – 5168; e) S. Wang, H. Sun, U. Ail, M. Vagin, P. O. Persson, J. W. Andreasen, W. Thiel, M. Berggren, X. Crispin, D. Fazzi, S. Fabiano, *Adv. Mater.* **2016**, *28*, 10764 – 10771; f) C. Y. Yang, W. L. Jin, J. Wang, Y. F. Ding, S. Nong, K. Shi, Y. Lu, Y. Z. Dai, F. D. Zhuang, T. Lei, C. A. Di, D. Zhu, J. Y. Wang, J. Pei, *Adv. Mater.* **2018**, *30*, e1802850; g) K. Yang, X. Zhang, A. Harbuzaru, L. Wang, Y. Wang, C. Koh, H. Guo, Y. Shi, J. Chen, H. Sun, K. Feng, M. C. Ruiz Delgado, H. Y. Woo, R. P. Ortiz, X. Guo, *J. Am. Chem. Soc.* **2020**, *142*, 4329 – 4340; h) X. Zhao, D. Madan, Y. Cheng, J. Zhou, H. Li, S. M. Thon, A. E. Bragg, M. E. DeCoster, P. E. Hopkins, H. E. Katz, *Adv. Mater.* **2017**, *29*, 1606928; i) Y. Lu, J.-Y. Wang, J. Pei, *Chem. Mater.* **2019**, *31*, 6412 – 6423.

[10] a) D. Fazzi, M. Caironi, C. Castiglioni, *J. Am. Chem. Soc.* **2011**, *133*, 19056 – 19059; b) G.-J. A. Wetzelaer, M. Kuik, Y. Olivier, V. Lemaur, J. Cornil, S. Fabiano, M. A. Loi, P. W. Blom, *Phys. Rev. B* **2012**, *86*, 165203; c) L. Zhang, B. D. Rose, Y. Liu, M. M. Nahid, E. Gann, J. Ly, W. Zhao, S. J. Rosa, T. P. Russell, A. Facchetti, *Chem. Mater.* **2016**, *28*, 8580 – 8590; d) B. J. Eckstein, F. S. Melkonyan, E. F. Manley, S. Fabiano, A. R. Mouat, L. X. Chen, A. Facchetti, T. J. Marks, *J. Am. Chem. Soc.* **2017**, *139*, 14356 – 14359.

[11] a) S. Wang, H. Sun, T. Erdmann, G. Wang, D. Fazzi, U. Lappan, Y. Puttisong, Z. Chen, M. Berggren, X. Crispin, A. Kiriy, B. Voit, T. J. Marks, S. Fabiano, A. Facchetti, *Adv. Mater.* **2018**, *30*, e1801898; b) H. Jia, T. Lei, *J. Mater. Chem. C* **2019**, *7*, 12809 – 12821.

[12] S. Wang, D. Fazzi, Y. Puttisong, M. J. Jafari, Z. Chen, T. Ederth, J. W. Andreasen, W. M. Chen, A. Facchetti, S. Fabiano, *Chem. Mater.* **2019**, *31*, 3395 – 3406.

[13] a) Y. Lu, Z. D. Yu, R. Z. Zhang, Z. F. Yao, H. Y. You, L. Jiang, H. I. Un, B. W. Dong, M. Xiong, J. Y. Wang, J. Pei, *Angew. Chem. Int. Ed.* **2019**, *58*, 11390 – 11394; *Angew. Chem.* **2019**, *131*, 11512 – 11516; b) H. Chen, M. Moser, S. Wang, C. Jellett, K. Thorley, G. T. Harrison, X. Jiao, M. Xiao, B. Purushothaman, M. Alsufyani, H. Bristow, S. De Wolf, N. Gasparini, A. Wadsworth, C. R. McNeill, H. Sirringhaus, S. Fabiano, I. McCulloch, *J. Am. Chem. Soc.* **2020**, *142*, 652 – 664.

[14] a) M. Alsufyani, R. K. Hallani, S. Wang, M. Xiao, X. Ji, B. D. Paulsen, K. Xu, H. Bristow, H. Chen, X. Chen, H. Sirringhaus, J. Rivnay, S. Fabiano, I. McCulloch, *J. Mater. Chem. C* **2020**, *8*, 15150 – 15157; b) K. Huang, G. Huang, X. Wang, H. Lu, G. Zhang, L. Qiu, *ACS Appl. Mater. Interfaces* **2020**, *12*, 17790 – 17798; c) D. Qu, T. Qi, H. Huang, *J. Energy Chem.* **2021**, *59*, 364 – 387; d) Z. Yuan, B. Fu, S. Thomas, S. Zhang, G. DeLuca, R. Chang, L. Lopez, C. Fares, G. Zhang, J.-L. Bredas, E. Reichmanis, *Chem. Mater.* **2016**, *28*, 6045 – 6049.

[15] J. Liu, Y. Shi, J. Dong, M. I. Nugraha, X. Qiu, M. Su, R. C. Chiechi, D. Baran, G. Portale, X. Guo, L. J. A. Koster, *ACS Energy Lett.* **2019**, *4*, 1556 – 1564.

[16] J. Liu, L. Qiu, R. Alessandri, X. Qiu, G. Portale, J. Dong, W. Talsma, G. Ye, A. A. Sengrian, P. C. T. Souza, M. A. Loi, R. C. Chiechi, S. J. Marrink, J. C. Hummelen, L. J. A. Koster, *Adv. Mater.* **2018**, *30*, 1704630.

[17] a) J. Liu, G. Ye, H. G. O. Potgieser, M. Koopmans, S. Sami, M. I. Nugraha, D. R. Villalva, H. Sun, J. Dong, X. Yang, X. Qiu, C. Yao, G. Portale, S. Fabiano, T. D. Anthopoulos, D. Baran, R. W. A. Havenith, R. C. Chiechi, L. J. A. Koster, *Adv. Mater.* **2020**, e2006694; b) D. Kiefer, A. Giovannitti, H. Sun, T. Biskup, A. Hofmann, M. Koopmans, C. Cendra, S. Weber, L. J. Anton Koster, E. Olsson, J. Rivnay, S. Fabiano, I. McCulloch, C. Muller, *ACS Energy Lett.* **2018**, *3*, 278 – 285.

[18] A. Babel, S. A. Jenekhe, *J. Am. Chem. Soc.* **2003**, *125*, 13656 – 13657.

[19] a) Y. Qiao, Y. Guo, C. Yu, F. Zhang, W. Xu, Y. Liu, D. Zhu, *J. Am. Chem. Soc.* **2012**, *134*, 4084 – 4087; b) F. Hinkel, J. Freudenberg, U. H. Bunz, *Angew. Chem. Int. Ed.* **2016**, *55*, 9830 – 9832; *Angew. Chem.* **2016**, *128*, 9984 – 9986; c) J. Hioe, D. Šakić, V. Vrček, H. Zipse, *Org. Biomol. Chem.* **2015**, *13*, 157 – 169.

[20] C.-Y. Yang, M.-A. Stoeckel, T.-P. Ruoko, H.-Y. Wu, X. Liu, N. B. Kolhe, Z. Wu, Y. Puttisong, C. Musumeci, M. Massetti, *Nat. Commun.* **2021**, *12*, 1 – 8.

[21] a) A. Onwubiko, W. Yue, C. Jellett, M. Xiao, H. Y. Chen, M. K. Ravva, D. A. Hanifi, A. C. Knall, B. Purushothaman, M. Nikolka, J. C. Flores, A. Salleo, J. L. Bredas, H. Sirringhaus, P. Hayoz, I. McCulloch, *Nat. Commun.* **2018**, *9*, 416; b) P. Singla, N. Van Steerteghem, N. Kaur, A. Z. Ashar, P. Kaur, K. Clays, K. S. Narayan, K. Singh, *J. Mater. Chem. C* **2017**, *5*, 697 – 708; c) N. M. Randell, P. C. Boutin, T. L. Kelly, *J. Mater. Chem. A* **2016**, *4*, 6940 – 6945; d) X. Chen, A. Marks, B. D. Paulsen, R. Wu, R. B. Rashid, H. Chen, M. Alsufyani, J. Rivnay, I. McCulloch, *Angew. Chem. Int. Ed.* **2021**, *60*, 9358 – 9373; *Angew. Chem.* **2021**, *132*, 9454 – 9459; e) Y. Deng, B. Sun, Y. He, J. Quinn, C. Guo, Y. Li, *Chem. Commun.* **2015**, *51*, 13515 – 13518.

[22] a) P. Wei, T. Menke, B. D. Naab, K. Leo, M. Riede, Z. Bao, *J. Am. Chem. Soc.* **2012**, *134*, 3999 – 4002; b) P. Wei, J. H. Oh, G. Dong, Z. Bao, *J. Am. Chem. Soc.* **2010**, *132*, 8852 – 8853.

[23] S. Riera-Galindo, A. Orbelli Biroli, A. Forni, Y. Puttisong, F. Tessore, M. Pizzotti, E. Pavlopoulou, E. Solano, S. Wang, G. Wang, *ACS Appl. Mater. Interfaces* **2019**, *11*, 37981 – 37990.

[24] A. Giovannitti, R. B. Rashid, Q. Thiburce, B. D. Paulsen, C. Cendra, K. Thorley, D. Moia, J. T. Mefford, D. Hanifi, D. Weiyuan, *Adv. Mater.* **2020**, *32*, 1908047.

[25] M. Moser, A. Savva, K. Thorley, B. D. Paulsen, T. C. Hidalgo, D. Ohayon, H. Chen, A. Giovannitti, A. Marks, N. Gasparini, A. Wadsworth, J. Rivnay, S. Inal, I. McCulloch, *Angew. Chem. Int. Ed.* **2021**, *60*, 7777 – 7785; *Angew. Chem.* **2021**, *133*, 7856 – 7864.

[26] S. Olthof, S. Mehraeen, S. K. Mohapatra, S. Barlow, V. Coropceanu, J.-L. Brédas, S. R. Marder, A. Kahn, *Phys. Rev. Lett.* **2012**, *109*, 176601.

[27] I. E. Jacobs, E. W. Aasen, J. L. Oliveira, T. N. Fonseca, J. D. Roehling, J. Li, G. Zhang, M. P. Augustine, M. Mascal, A. J. Moulé, *J. Mater. Chem. C* **2016**, *4*, 3454 – 3466.

[28] V. Dusastre, *Materials for sustainable energy: a collection of peer-reviewed research and review articles from Nature Publishing Group*, World Scientific, **2010**.

[29] D. De Leeuw, M. Simenon, A. Brown, R. Einerhand, *Synth. Met.* **1997**, *87*, 53 – 59.